# Binding and Electron Transfer between Putidaredoxin and Cytochrome P450cam. Theory and Experiments

**Adrian E. Roitberg,* Marcia J. Holden, Martin P. Mayhew, Igor V. Kurnikov,† David N. Beratan,† and Vincent L. Vilker**

*Contribution from the Biotechnology Division, National Institute of Standards and Technology, Building 222, Room A353, Gaithersburg, MD 20899*

*Received November 24, 1997*

**Abstract:** We present a detailed atomic level view of the interactions between cytochrome P450cam (CYP101) and its natural redox partner, putidaredoxin (Pdx). A combined theoretical (Poisson−Boltzmann electrostatic calculations, electron transfer pathways, and molecular dynamics) and experimental (site-directed mutagenesis and kinetic analysis) study is used to pinpoint surface residues in both proteins that are important for electron transfer, binding, or both. We find a situation where the electrostatically complementary regions at the surface of both proteins overlap strongly with regions that have large electron transfer couplings to the redox centers. This means that a small surface patch in each protein is involved in binding and electron transfer. A dominant electron transfer pathway is identified, corresponding to an electron leaving the reduced $Fe_2S_2$ in Pdx, going through Cys39 and Asp38, and transferring across the interprotein interface to Arg112 (CYP101), then to a heme propionate group, and finally to the heme iron center.

## Introduction

A necessary step in understanding biological function in multiple metalloprotein redox systems is the description of protein−protein binding and electron transfer between two distant metal centers. In this paper, we present experimental and theoretical analyses of the residues that are involved in the binding and the electron transfer pathways of the cytochrome P450cam (CYP101) and putidaredoxin (Pdx) protein complex.

The in vivo function of the CYP101 enzymatic complex is to catalyze the stereoselective oxidation of camphor to 5-*exo*-hydroxycamphor. The bacterium *Pseudomonas putida*, from which this enzyme was originally extracted and purified, can survive by using camphor as its sole carbon and energy source.[1] The full catalytic cycle of CYP101 starts with NADH, which reduces the FAD-containing protein putidaredoxin reductase (PdR). PdR then transfers an electron to putidaredoxin (Pdx). Two distinct electron transfer steps are needed from Pdx to CYP101 in order to enable catalysis. The first electron transfer step can be attained by a number of compounds, but the second one can only be done in the presence of Pdx. The origin of this difference in behavior is yet to be resolved, and in the present paper, we will not distinguish between these two steps. It is however important to note that there is probably a single binding site associated with each of the independent electron transfer events.[2,3]

Of the three proteins in this cycle, only the structure of CYP101 (MW 45 000) has been elucidated using X-ray methods.[4,5] A solution structure of Pdx (MW 11 594) has been elucidated using NMR methods[6] and deposited in the PDB[7] database under the code 1PUT. It is worth noting that the NMR experiments on this protein are hampered by the presence of the paramagnetic $Fe_2S_2$ cluster. This fact has the effect of largely displacing and grossly widening the NMR lines for most nuclei lying within an 8 Å sphere of the cluster. The route followed by Pochapsky consisted of collecting the largest possible number of NOE restraints and dihedral restraints and a number of paramagnetic broadening restraints. There are also data to support the idea that the regions close to the metallic cluster are homologous among a series of ferredoxins. The large homology between Pdx and the ferredoxins of *Spirulinas platensis* and *Anabaena* at the cluster region enabled Pochapsky to model the active site region. The mix of homology section and the actual NMR data were then minimized with the usual methodologies.[6] The stability of that structure when immersed in a box of water with proper inclusion of electrostatic terms has been recently studied,[8] and it was found that the structure proposed by Porchapsky holds very well under long molecular dynamics conditions. Very recently, an X-ray structure of a highly homologous protein has been solved;[9] a truncated bovine adrenodoxin was elucidated at a resolution of 1.85 Å and has a main-chain RMSD deviation to Pdx of only 1.64 Å. Recently, Pochapsky et al.[10] proposed a model for the structure of the Pdx−CYP101 complex based on molecular dynamics simulations that attempted to place the iron−sulfur center of Pdx as

* To whom correspondence should be addressed. E-mail: adrian@nist.gov.
† Department of Chemistry, University of Pittsburgh, Pittsburgh, PA 15260.

(1) Ortiz de Montellano, P. R. *Cytochrome P450*: *structure, mechanism, and biochemistry*, 2nd ed.; Plenum Press: New York,1995.
(2) Hintz, M. J.; Mock, D. M.; Peterson, L. L.; Tuttle, K.; Peterson, J. A. *J. Biol. Chem.* **1982**, *257*, 14324.
(3) Unno, M.; Shimada, H.; Toba, Y.; Makino, R.; Ishimura, Y. *J. Biol. Chem.* **1996**, *271*, 17869−17874.
(4) Poulos, T. L.; Finzel, B. C.; Howard, A. J. *J. Mol. Biol.* **1987**, *195*, 687.
(5) Poulos, T. L.; Raag, R. *FASEB J.* **1992**, *6*, 674−679.
(6) Pochapsky, T. C.; Ye, X. M.; Ratnaswamy, G.; Lyons, T. A. *Biochemistry* **1994**, *33*, 6424−6432.
(7) Bernstein, F. C.; Koetzle, T. F.; Williams, G. J. B.; Meyer, J. E. F.; Brice, M. D.; Rodgers, J. R.; Kennard, O.; Shimanouchi, T.; Tasumi, M. *J. Mol. Biol.* **1977**, *112*, 535−542.
(8) Roitberg, A. E. *Biophys. J.* **1997**, *73*, 2138−2148.
(9) Muller, A.; Muller, J. J.; Muller, Y. A.; Uhlmann, H.; Bernhardt, R.; Heinemann, U. *Structure* **1998**, *6*, 269−280.

S0002-7863(97)03990-5 CCC: $15.00 © 1998 American Chemical Society
Published on Web 08/21/1998

close as possible to the heme group of CYP101.[10] They identified a number of ionic bridges and aromatic−aromatic interactions being present at the interface between the two proteins with the redox centers separated by 12 Å.

A large amount of experimental evidence has been gathered over the years regarding the binding and electron transfer events in this system, although no complete, atomic level picture of these two events has yet been proposed and tested. Site-directed mutagenesis has been used to pinpoint surface residues that possibly take part in either the binding or the electron transfer event, with some residues identified as being important for both.[3,11,12] Sligar et al. showed that, contrary to initial considerations, Trp106 (Pdx) is involved in binding but not in electron transfer.[11] Others have shown that Arg112 (CYP101) is important for both electron transfer and binding.[3] More recently, our group conducted extensive mutagenesis experiments on surface residues on Pdx.[12] From these experiments, a picture emerged that points to Asp38 on Pdx as the most important residue in electron transfer and binding between the target proteins, with Asp34 (Pdx) providing a role in binding only. Now, we present details of the theoretical and experimental methodologies used to complete an atomic picture of the binding interface of Pdx and CYP101, as well as a description of those residues involved in electron transfer. A Poisson−Boltzmann treatment was used as an aid to understanding the electrostatic effects on binding and complex formation, while a pathways model was used to identify surface residues with likely roles in electron transfer. Moreover, we modeled the protein−protein complex, using a molecular dynamics approach to rationalize the overall picture emerging from the data. Experimental data were obtained on a series of site-directed mutations on Pdx and CYP101, followed by kinetic measurements of electron transfer ($V_{max}$) and binding ($K_m$) related constants. The residues that have been mutated were chosen on the basis of expectations regarding structure and function, but two of the mutations (Leu356 in CYP101 and Ser44 in Pdx) were chosen directly as a result of the theoretical calculations, which pointed to them as possible electron transfer sites.

## Methods

**Theory. (a) Electrostatic Poisson−Boltzmann Calculations.** The electrostatic calculations were performed by iterating the finite difference solution of the linearized Poisson−Boltzmann (PB)[13−16] equation as implemented in a locally modified version of the program UHBD.[17] The protein dielectric constant was set to 2, while the solvent was assumed to be water and thus its dielectric constant was 78. The temperature was 300 K, the ionic strength 150 mM, and the Debye−Huckel parameter 0.127 Å$^{-1}$. A 1 Å spaced grid of 65$^3$ size was used for all calculations. Amino acid charges where taken from the CHARMM force field. Electrostatic potential contours were drawn at −2 kcal/(mol e) (red) and +2 kcal/(mol e) (blue) computed for Pdx (Figure 1a) and CYP101 (Figure 1b).

**(b) Pathways Electron Transfer Analysis.** As a second component of the analysis, the pathway method for predicting electron-coupling routes was used. The basic underlying assumption is that the dominant electron transfer tunneling route will be one that will take an electron with maximum coupling from the $Fe_2S_2$ center in Pdx to some atom in its surface, jump through space to the nearest atom in CYP101, and from there find a route to the heme group in CYP101. We briefly describe the basis of the pathways method, and its detailed representation when used for interprotein electron transfer. The explanation below has been adapted from that given in ref 18.

The nonadiabatic formulation of electron transfer rates can be written in a Fermi Golden Rule form:[19]

$$k_{ET} = (2\pi/\hbar)|T_{DA}|^2(FC) \tag{1}$$

with $|T_{DA}|^2$ being the electronic tunneling matrix element between putative donor and acceptor sites and FC is the Franck−Condon factor describing a nuclear factor relating the driving force and reorganization energy for the reaction. In the case of medium assisted electron transfer, it is of primary importance to understand, even qualitatively, how $|T_{DA}|^2$ is modulated by the structure and dynamics of the bridge.[20−22] In the case of proteins, a powerful approximate method was introduced by Beratan and Onuchic.[23−28] This method differentiates among through bond, through space, and through H-bond electronic couplings, producing an approximation to $T_{DA}$ of the form

$$T_{DA} = C\prod_b \epsilon_b \prod_h \epsilon_h \prod_s \epsilon_s \tag{2}$$

where $C$ is a prefactor, and the products run over bonds, hydrogen bonds, and through space connections, respectively. The $\epsilon$ values represent decay parameters for the electronic coupling associated with bonds, space, and H-bonds according to their subscripts. Following the prescribed method, the values for the decay parameters are taken as[23−25]

$$\epsilon_b = 0.6 \tag{3}$$

$$\epsilon_h = {\epsilon_b}^2 \exp[-1.7(d - 2d_b)] \tag{4}$$

$$\epsilon_s = 0.5\epsilon_b \exp[-1.7(d - d_b)] \tag{5}$$

with $d$ being an intercenter distance (Å), and $d_b$ a reference covalent distance (1.4 Å). The decay factors are unitless. When donor and acceptor centers are identified, a path is chosen such that $T_{DA}$ in eq 2 is maximized.

For interprotein electron transfer, the product of eq 2 is expressed in a different way:[18]

$$T_{DA} = C\prod_D \epsilon_D \prod_A \epsilon_A \epsilon_{inter} \tag{6}$$

In this case, the first product in eq 6 is taken over paths in the electron donor protein and the second product over the electron acceptor protein, with the third term representing the decay factor associated with the electron coupling across the protein−protein interface (usually through

(10) Pochapsky, T. C.; Lyons, T. A.; Kazanis, S.; Arakaki, T.; Ratnaswamy, G. *Biochimie* **1996**, *78*, 723−733.
(11) Davies, M. D.; Sligar, S. G. *Biochemistry* **1992**, *31*, 11383−11389.
(12) Holden, M.; Mayhew, M.; Bunk, D.; Roitberg, A.; Vilker, V. *J. Biol. Chem.* **1997**, *272*, 21720−21725.
(13) Honig, B.; Nicholls, A. *Science* **1995**, *268*, 1144−1149.
(14) Nicholls, A.; Honig, B. *J. Comput. Chem.* **1991**, *12*, 435−445.
(15) Gilson, M. K.; Honig, B. H. *Proteins*: *Struct. Funct. Genet.* **1988**, *3*, 32−52.
(16) Gilson, M. K.; Rashin, A.; Fine, R.; Honig, B. *J. Mol. Biol.* **1985**, *184*, 503−516.
(17) Madura, J. D.; Briggs, J. M.; Wade, R. C.; Davis, M. E.; Luty, B. A.; Ilin, A.; Antosiewicz, J.; Gilson, M. K.; Bagheri, B.; Scott, L. R.; McCammon, J. A. *Comput. Phys. Commun.* **1995**, *91*, 57−95.
(18) Aquino, A. J. A.; Beroza, P.; Beratan, D. N.; Onuchic, J. N. *Chem. Phys.* **1995**, *197*, 277−288.
(19) Marcus, R. A. *J. Chem. Phys.* **1956**, *43*, 679.
(20) Bertrand, P. *Long-range electron transfer in biology*; Springer-Verlag: Berlin, New York, 1991.
(21) Curtiss, L. A.; Naleway, C. A.; Miller, J. R. *J. Phys. Chem.* **1993**, *97*, 4050−4058.
(22) Closs, G. L.; Miller, J. R. *Science* **1988**, *240*, 440−447.
(23) Beratan, D. N.; Onuchic, J. N.; Hopfield, J. J. *J. Chem. Phys.* **1987**, *86*, 4488−4498.
(24) Beratan, D. N.; Betts, J. N.; Onuchic, J. N. *Science* **1991**, *252*, 1285−1288.
(25) Onuchic, J. N.; Beratan, D. N. *J. Chem. Phys.* **1990**, *92*, 722−733.
(26) Onuchic, J. N.; de Andrade, P. C. P.; Beratan, D. N. *J. Chem. Phys.* **1991**, *95*, 1131−1138.
(27) Onuchic, J. N.; Beratan, D. N.; Winkler, J. R.; Gray, H. B. *Annu. Rev. Biophys. Biomol. Struct.* **1992**, *21*, 349−377.
(28) Regan, J. J.; Risser, S. M.; Beratan, D. N.; Onuchic, J. N. *J. Phys. Chem.* **1993**, *97*, 13083−13088.

space or H-bonds). The first two terms consist of decays of any of the types described in eqs 3−5, and are well defined provided a set of coordinates for the system is available. $\epsilon_{inter}$, on the other hand, is dependent on the details of the interface geometry, and hence the less reliable of these quantities. We have chosen a route similar to that used in refs 18 and 29, where a coupling map is computed from the donor (acceptor) site within the donor (acceptor) protein to each atom in the protein surface. Figure 2 shows the result of such calculations for Pdx and CYP101. All figures were prepared using the program GRASP.[30]

**(c) Docking.** A molecular dynamics run was performed (in vacuo) to attempt to model the Pdx−CYP101 complex at an atomic level, with the idea of providing a playing field to interpret the results from the electrostatic and pathways analysis calculations, plus the experimental results. The program Amber (version 4.1)[31] was used for all simulations. A soft harmonic restraint with a force constant of 2 kcal/(mol Å$^2$) was set between the iron atom closest to the Pdx surface and the iron atom in the heme group in CYP101. The initial value of the distance restraint was set to 40 Å, and a molecular dynamics run of 50 ps was performed to equilibrate the system at 300 K. Then, the value of the equilibrium distance restraint was reduced in decrements of 5 Å every 50 ps, and then by 1 Å every 50 ps up to 12 Å. (Some details of the protocol can be found at http://www.amber.uscf.edu/amber/Questions/docking.html). The effect of this simulation is to reduce the system to a single rotation around the iron−iron axis. This protocol is essentially the same followed by Pochapsky et al.[10] This simulation was run five times from different initial conditions with results that were essentially the same for all repetitions.

**Experiment.** Wild type and mutant Pdx and CYP101 proteins were heterologously expressed in *E. coli* (DH5α) cells carrying a plasmid containing the gene for Pdx or CYP101 and subsequently purified as described in Grayson et al.[32] In brief, the cells were grown in batch culture in a rich medium and lysed by freeze−thaw with the addition of lysozyme and DNase. Pdx protein was purified using two chromatographic steps. Pdx was eluted from a DEAE fast flow sepharose column (Pharmacia Biotech, Uppsala, Sweden) with a gradient of KCl. The protein was concentrated and chromatographed on a gel filtration column. The final protein product was >99% pure. Complete purification of CYP101 required, in addition to the previous two steps, a hydrophobic interaction chromatography step not previously described. The 2.5 cm × 10 cm column (phenyl sepharose 6 fast flow, Pharmacia Biotech, Uppsala, Sweden) was equilibrated with a buffer of 50 mM $Na_3PO_4$, pH 7.4, with 1 M $(NH_4)_2SO_4$. Ammonium sulfate was also added to the protein solution to a final concentration of 1 M. After the protein was loaded onto the column, the column was washed with the equilibration buffer, and then a two-step gradient was run. The first step consisted of 100 mL of 1−0.2 M $(NH_4)_2SO_4$ in the phosphate buffer. This was followed by a 200 mL gradient of 0.2−0 M $(NH_4)_2SO_4$. Site-directed mutagenesis was carried out using commercially available kits (Transformer Site-Directed Mutagenesis, Clontech, Palo Alto, CA; QuickChange site-directed mutagenesis, Stratagene, LaJolla, CA). DNA primers, used in the mutagenesis reactions, were commercially synthesized. The mutated genes were sequenced using dye-terminator chemistry on an Applied Biosciences Model 373 sequencer. Further verification of the mutation was accomplished with the determination of the molecular mass of the protein using electrospray mass spectrometry. The above protocols were described in Holden et al.[12] The mutant species are identified by the one-letter symbol for the mutated position followed by the identity of the new amino acid, e.g., L356A (alanine has been substituted for the leucine at position 356 of CYP101). Activity assays and kinetic analyses were conducted as described in Holden et al.[12].

## Results and Discussion

**Theory.** The results obtained using the methodologies described in the previous section can be interpreted in terms of residues involved in binding and/or electron transfer between the two proteins involved in this study. From a theoretical point of view, the Poisson−Boltzmann (PB) electrostatic calculations can be thought of as providing an inroad into the role of certain residues in binding. The involvement of electrostatic effects in protein−protein binding has been extensively discussed in the literature. In the case of Pdx-CYP101, it has been reported that the binding constant is substantially reduced upon an increase in ionic strength.[2] In particular, Unno et al.[33] have shown inhibition of complex formation in 0.5 M NaC1 solution. This points to a substantial role of electrostatics in binding. This effect has been found before in a number of systems such as cytochrome $c_2$−photosynthetic reaction center,[34] plastocyanin−cytochrome *f*,[35] and cytochrome *c*−cytochrome *c* peroxidase.[36,37]

A PB calculation on Pdx (Figure 1a) shows as a unique feature the presence of a triangular patch of contiguous negative electrostatic potential (red contour at −2 kcal/(mol e)). The three vertices of this triangle are D34, D38, and W106 (the latter being the C-terminal residue and hence negatively charged). No other regions of contiguous negative or positive potential are found in Pdx, and hence the aforementioned triangle will be interpreted as the most likely site involved in binding. Previous work with CYP101[38,39] identified a surface region of 20 Å diameter centered around the heme group in CYP101 that can be assigned a positive potential. We further identify patches of positive electrostatic potential contours (blue at +2 kcal/(mol e)) overlapping with arginine and lysine residues in the proximal face of CYP101 (face closest to the heme group). Figure 1b shows that the complete back side (surface opposite the proximal face of CYP101) of CYP101 is a continuous region of negative potential (red = −2 kcal/(mol e) contour). This means that at least half of CYP101's surface can be excluded as a binding site for Pdx.

The pathways model of electron transfer was used to pinpoint surface residues that have large couplings to the redox centers in their respective proteins. Figure 2a shows such couplings projected into the surface of Pdx, with the coloring proportional to log $|T_{DA}|^2$, red colors representing large couplings and blue colors representing very small couplings. There are atoms corresponding to only two residues that show large couplings to the $Fe_2S_2$ cluster and are solvent exposed. These are $H_G$ in Ser44 and $O_{D1}$ ($O_{D2}$) in Asp38. Their log $|T_{DA}|^2$ values, computed as in eq 2 (with a value of $C$ equal to 1) is −3.99. Figure 2b presents the values of log $|T_{DA}|^2$ for coupling between the heme group and solvent-exposed residues in CYP101. Again, only atoms corresponding to two residues show large couplings: the H atoms attached to the solvent-exposed $N_H$ in Arg112 (log $|T_{DA}|^2 = -3.78$) and the H atoms bonded to $C_{D1}$ and $C_{D2}$ in Leu356 (log $|T_{DA}|^2 = -4.44$). For completeness, we note that the other two residues in Pdx that were flagged as possible binding sites (D34 and W106) have extremely small couplings to the $Fe_2S_2$ cluster (log $|T_{DA}|^2 = -9.32$ and −10.05, respectively) and hence will play no role in electron transfer. A naive view of electron transfer would attempt to place the

(29) Nocek, J. M.; Zhou, J. S.; DeForest, S.; Priyadarshy, S.; Beratan, D. N.; Onuchic, J. N.; Hoffman, B. M. *Chem. Rev.* **1996**, *96*, 2459−2489.
(30) Nicholls, A.; Sharp, K. A.; Honig, B. *Proteins* **1991**, *11*, 281−96.
(31) Pearlman, D. A.; Case, D. A.; Caldwell, J. W.; Ross, W. S.; Cheatham, T. E.; Debolt, S.; Ferguson, D.; Seibel, G.; Kollman, P. *Comput. Phys. Commun.* **1995**, *91*, 1−41.
(32) Grayson, D. A.; Tewari, Y. B.; Mayhew, M. P.; Vilker, V. L.; Goldberg, R. N. *Arch. Biochem. Biophys.* **1996**, *332*, 239−247.
(33) Unno, M.; Christian, J. F.; Benson, D.; Gerber, N.; Sligar, S. G.; Champion, P. M. *Biophys. J.* **1996**, *70*, WP335−WP335.
(34) Moser, C. C.; Dutton, P. L. *Biochemistry* **1988**, *27*, 2450−2461.
(35) Ullmann, G. M.; Knapp, E. W.; Kostic, N. M. *J. Amer. Chem. Soc.* **1997**, *119*, 42−52.
(36) Pelletier, H.; Kraut, J. *Science* **1992**, *258*, 1748−1755.
(37) Poulos, T. L.; Kraut, J. *J. Biol. Chem.* **1980**, *255*, 1748−1755.
(38) Rodgers, K. K.; Sligar, S. G. *J. Mol. Biol.* **1991**, *221*, 1453−1460.
(39) Stayton, P. S.; Poulos, T. L.; Sligar, S. G. *Biochemistry* **1989**, *28*, 8201−8205.

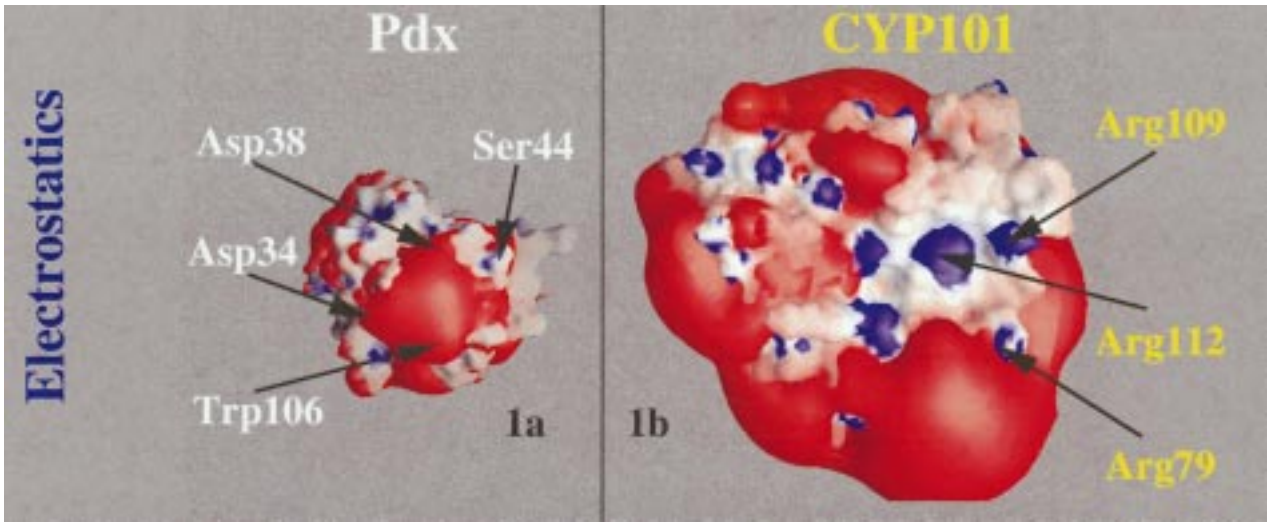


**Figure 1.** Poisson−Boltzmann electrostatic calculations. (a) Electrostatic contour plots (red = −2 kcal/(mol e)) for Pdx. (b) Electrostatic contour plots (red = −2 kcal/(mol e), blue = +2 kcal/(mol e)) for CYP101. There is a triangular region in Pdx comprised of residues Asp34 and Asp38 and the C- terminal residue Trp106 of negative potential, and patches of positive potential in the proximal face of CYP101.

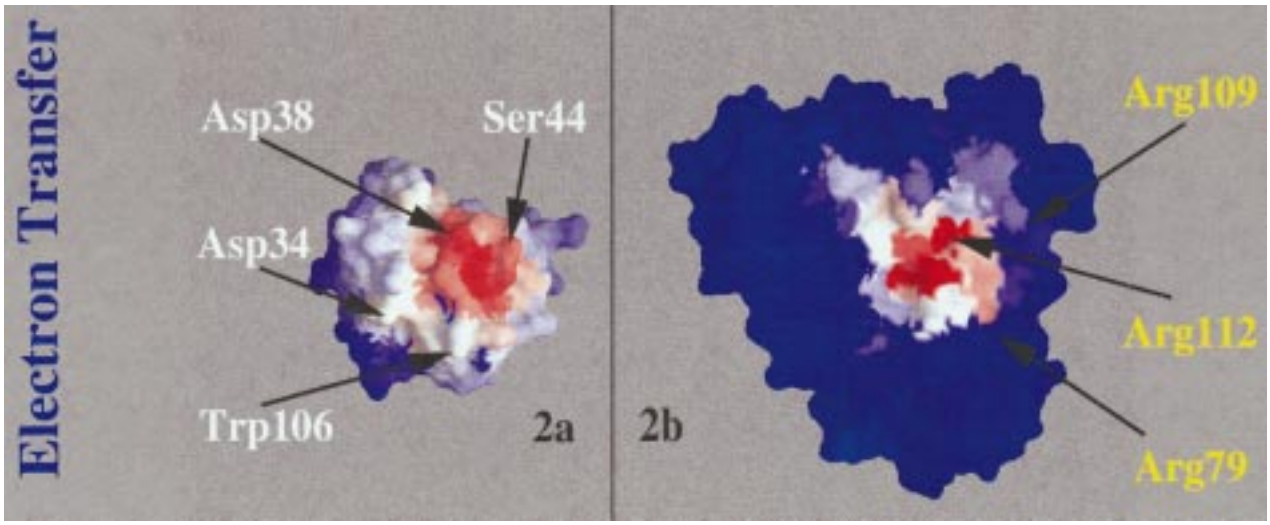


**Figure 2.** Pathways analysis of electron transfer. (a) Coupling between the $Fe_2S_2$ center in Pdx and surface residues as log $|\prod_i \epsilon_i|^2$. (b) Coupling between the heme group in CYP101 and surface residues as log $|\prod_i \epsilon_i|^2$. Red and blue represent large and very small couplings, respectively. There are two residues in each protein with large couplings (Asp38 and Ser44 in Pdx, and Arg112 and Leu356 in CYP101).

atoms with large coupling in each protein close to each other, so as to minimize the interprotein electron transfer coupling decay across the interface. If the regions of large couplings in both proteins are extensive, then a picture emerges where the sensitivity of electron transfer rates to conformational changes is minor. If, as in this case, the regions of large couplings are very narrow (in fact, of atomic detail), then a strong argument can be made for these sites to be involved with a particular geometry of the protein−protein complex that will maximize the electronic coupling. We need to emphasize that the geometry conformation most favorable for electron transfer need not be the most stable thermodynamically. There are examples in the literature where the ET active geometry is not the most stable,[29,35] but we will show that in the particular case treated here the opposite mechanism seems to be at play.

A molecular dynamics simulation was performed as described in the Methods, and yielded a stable complex every time the procedure was run. The method employed here to dock the two proteins makes use of a number of previous results, and allows us to start from relative orientations that are close to the final one. In the general case, one must do a more complete search of the available confirmational space in the manner described by Ullmann et al.[35] The complex obtained buries 700 Å$^2$ of surface area per protein and agrees fairly well with the results described by Pochapsky.[10] Figure 3 presents a view of the complex obtained with the MD runs, with the interface region expanded. The fit is extremely good and puts the two redox centers at a distance of 12 Å. This arrangement of the two proteins is such that the individual dipole moments are aligned. This effect has been mentioned before as possibly helping reduce the entropic problem in protein−protein orientation and steering proteins toward their preferred relative orientations.[40,41] In the magnification of the binding interface, residues labeled "C" correspond to CYP101 and residues labeled "P" to Pdx. There are a number of important facts arising from the atomic level view of the complex. Three ionic bridges (shown as dashed green lines) are formed between positively charged residues in CYP101 (Arg79, Arg109, and Arg112) and three residues in Pdx (Asp34, Asp38, and Trp106). There is also an H-bond (in purple) in Figure 3 associated with the contact between the guanidino group in Arg112 and the O atom

(40) Janin, J. *Proteins: Struct. Funct., Genet.* **1997**, *28*, 153−161.
(41) Harris, T. K.; Davidson, V. L.; Chen, L. Y.; Mathews, F. S.; Xia, Z. X. *Biochemistry* **1994**, *33*, 12600−12608.

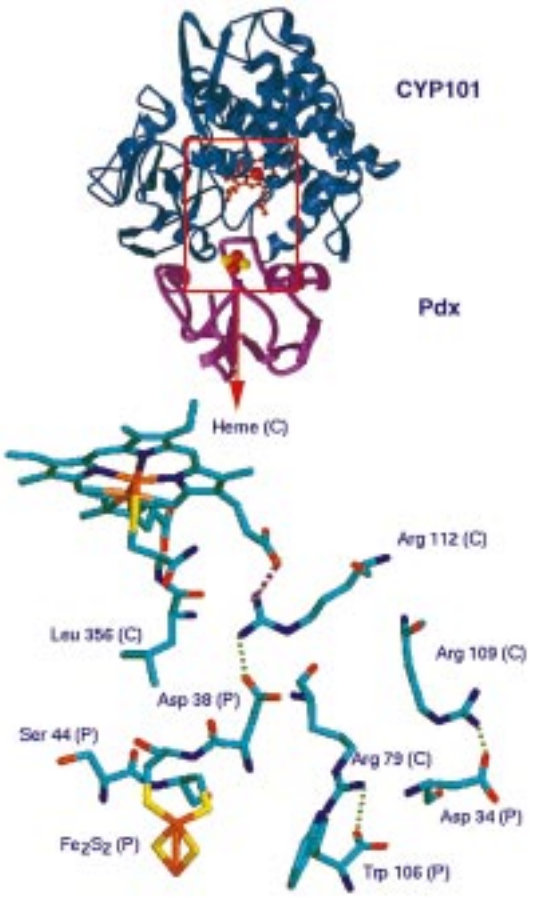


**Figure 3.** Geometry of the Pdx−CYP101 complex and expansion of the binding contact showing residues at the interface. There are three ionic bridges responsible for binding.

of 6-propionate of the iron protoporphyrin. Residues Asp34, Asp38, and Trp106 of Pdx correspond to the vertices of the triangle found with the Poisson−Boltzmann electrostatic calculations in Figure 1a, while the three residues in CYP101 are three of the electrostatically positive features found in CYP101-in Figure 1b. One of the ionic bridges is of primary importance because it puts within a short distance two residues, one in each protein, that have maximal electron transfer coupling with their respective redox centers (Arg112 in CYP101 and Asp38 in Pdx). Also, the two other groups that where flagged as possible electron transfer surface residues (Ser44 in Pdx and Leu356 in CYP101) in Figure 2 are relatively close to each other and could potentially be part of a second pathway. Only experimental observations can assess the relative strength of these two pathways.

Theory hence predicts a double role for Arg112 (CYP101) and for Asp38 (Pdx) as mediators for both binding (as electrostatically important residues) and electron transfer (as pinpointed by the pathways model). At the same time, Asp34 (Pdx) and Trp106 (Pdx) are predicted to be relevant only for binding, while Ser44 (Pdx) and Leu356(CYP101) could be important for electron transfer but not for binding.

**Experiment.** We have used site-directed mutagenesis to identify surface amino acid residues of Pdx and CYP101 that are important in binding and/or electron transfer. Mutations of the CYP101 subunit were directed to Leu356 that was changed to alanine while mutations on Pdx include Ser44 and Asp38, both possible electron transfer pathway components, and Asp34 as one of the three possible salt bridge residues (along with Asp38). All of the mutations (D34N, D38N, D38I, S44G, L356A) were verified by determination of molecular mass of the protein by electrospray mass spectrometry as well as by sequencing the DNA. Prior to kinetic analysis, we asked the question of whether the mutation at Leu356 of CYP101 affected the active site for camphor hydroxylation by measuring both NADH oxidation (spectrophotometer) and camphor hydroxylation (GC). The coupling of NADH oxidation with camphor hydroxylation was >95% for both the L356A mutant and WT CYP101. We also made use of related data obtained by Unno et al. regarding mutations at the Arg112 (CYP101) site.[3]

**Table 1.** Cytochrome P450cam Activity of Mutant and Wild Type Pdx and CYP101 Proteins[a]

| protein constituents | turnover (nmol of NADH·nmol of $CYP101^{-1}\cdot s^{-1}$) | % wild type activity |
|---|---|---|
| WT Pdx−WT CYP101 | 14.2 (0.4) | 100 |
| S44C Pdx−WT CYP101 | 12.6 (0.8) | 84 |
| WT Pdx−L356A CYP101 | 14.3 (0 7) | 100 |
| S44C Pdx−L356A CYP101 | 10.6 (0.5) | 75 |
| D38N Pdx−WT CYP101[12] | 1.1 (0 1) | 8 |
| D38I Pdx−WT CYP101[12] | 0.04 (0 2) | <1 |
| D34N Pdx−WT CYP101[12] | 9.1 (0.3) | 70 |
| protein constituents | turnover (nmol of $O_2$ consumed·nmol of $CYP101^{-1}\cdot s^{-1}$) | % wild type activity |
| WT Pdx−WT CYP101[3] | 21.7 | 100 |
| WT Pdx−R112K CYP101[3] | 3.3 | 15 |
| WT Pdx−R112C CYP101[3] | 0.02 | <1 |
| WT Pdx−R112M CYP101[3] | 0.03 | <1 |
| WT Pdx−R112Y CYP101[3] | 0.01 | <1 |

[a] Assays were run as described in Holden et. al.[12] To the combinations of mutant and WT protein (Pdx, CYP101) were added putidaredoxin reductase, NADH, and camphor. The oxidation of NADH was followed at 340 nm. Data from our previous work[12] and from Unno et al.[3] are included for comparative purposes. Numbers in parentheses are 1 SD. The data for $O_2$ consumption rates were recalculated from Table I of ref 3 to units equivalent to ours.

The rate of NADH oxidation by the complete CYP101 system (Pdx, PdR, CYP101) was used to measure the activity of mutant and wild type (WT) protein combinations. The measurements done with the D38N, D34N, and S44C Pdx mutants reflect only on the nature of the interactions of Pdx with CYP101 because other assays measuring the reduction of the mutant Pdx species by PdR gave the same values as did WT Pdx (ref 12 or data not shown). The D38I mutant was the only exception to this rule and shows reduced activity with PdR also.[12] Of the mutants that we have analyzed, the mutations of Asp38 (Pdx) caused the greatest loss of activity (Table 1). Conversion of Asp38 to asparagine resulted in loss of the charge on the side chain and reduction in activity to 8% of WT Pdx, while conversion of Asp38 to isoleucine essentially eliminated activity. In contrast, the mutation of Asp34 to asparagine and Ser44 to cysteine showed a much smaller loss of activity, 70% and 84% of WT Pdx activity, respectively. The L356A mutation of CYP101, which shortens the side chain from three to one carbon, has no effect on activity. Table 1 also relates equivalent data of Unno et al.[3] which shows that substitutions to arginine at position 112 of CYP101 have drastic effects. Even in the substitution of lysine, which maintains the charge resulted in the loss of 85% of activity with other substitutions, substituting uncharged side chains, all activity was lost. The above data indicate that there is a clear difference between the activities of the mutants associated with the two possible ET pairs. The large effect of mutations at the Asp38−Arg112 sites contrasts with the minor effect resulting from mutating the Ser44−Leu356 pair.

**Table 2.** Oxidation of Reduced Pdx by CYP101 and Camphor[a]

| protein constituents | turnover | % wild type activity |
|---|---|---|
| WT Pdx−WT CYP101 | 19.2 (3.8) | 100 |
| S44C Pdx−WT CYP101 | 17.2 (3.8) | 89.6 |
| WT Pdx−L356A CYP101 | 21.6 (2.0) | 112.5 |
| S44C Pdx−L356A CYP101 | 14.9 (0.3) | 77.6 |

[a] Pdx was prereduced by incubation with catalytic amounts of putidaredoxin reductase and NADH (equimolar to Pdx) as described in Holden et al.[12] Reoxidation is initiated by addition of CYP101 and camphor. The oxidation of Pdx is observed at 455 nm. Assays were conducted with WT CYP101 and Pdx at the same time as the mutant species. Numbers in parentheses are 1 SD.

Other analyses were completed in order to describe the effect of the mutations. The reoxidation of reduced Pdx by camphor and CYP101 is shown in Table 2. The rates shown here reflect only enzymatic oxidation, having been corrected for the small amount of nonenzymatic oxidation. The activities of the mutants as compared to the WT proteins are consistent with what was observed with the complete reaction (Table 1). L356A behaved as did the WT CYP101 while the S44C Pdx mutant had somewhat lower activity. A second mutation was done at Ser44 wherein a glycine was substituted for serine. This mutation resulted in a 16-fold increase in the rate of nonenzymatic reoxidation of reduced Pdx. This effect interfered with reasonable enzymatic analysis of any other effects of this mutation on activity. But the high nonenzymatic reoxidation rate of this mutation suggests that the serine side chain protects the Fe−S center of Pdx from external oxygen.

Even though the trends of overall activity correlate with the theoretical expectations, it remains to be explained if the role of those residues whose mutations decrease the activity do so because of electron transfer or binding effects. In order to distinguish such effects, we determined $K_m$ and $V_{max}$ of Pdx for CYP101 (Table 3). Correlation of $K_m$ with binding and $V_{max}$ with electron transfer rates has been previously performed by Sligar et al.[42] Only the $K_m$ of S44C was substantially increased, not the $V_{max}$, suggesting that this mutation caused a small decrease in the affinity of Pdx for CYP101 but had no effect on electron transfer rates. While the D38N mutant had a $K_m$ of 5.96 $\mu$M (versus 0.30 $\mu$M for WT Pdx) and a much reduced $V_{max}$, the D34N mutant had a $K_m$ of 0.65 $\mu$M and no change in $V_{max}$. This supports the theoretical analyses suggesting that Asp38 may play two roles, that of binding via a salt bridge as well as a pathway for electron transfer. The experimental results show that changes to Asp38 do more to affect the interaction of Pdx and CYP101 than changes to either Asp34, another salt bridge participant, or Ser44, a component of the other possible electron transfer pathway. Similarly the Arg112 mutations of CYP101 exhibited greatly reduced electron rate constants ($K_{et}$) and elevated binding constants ($K_d$)[3] (Table 3).

The combined result from theory and experiments allows us to present a detailed atomic model for the interaction of putidaredoxin and CYP101. Residues at the protein−protein interface are tagged as being important for binding and/or electron transfer, and we predict a possible electron transfer pathway. Both the pathway theoretical model and experimental approaches predict crucial roles for Asp38 (P) and Arg112 (C) in electron transfer and binding. The fact that the molecular dynamics model (ours and ref 9) for the interaction of these proteins allows for close contact and ionic binding for those residues is encouraging and points to a possible electron pathway. In this model, an electron would leave the $Fe_2S_2$ cluster in putidaredoxin, pass through Cys39 (P) (one of the four cysteine ligands for the active site), then tunnel through Asp38 (P), and jump across the protein−protein interface to Arg112 (C). From this residue, a single through space jump leads the electron directly to the heme group and completes the electron transfer step. The Ser44−Leu356 couple could also provide a pathway for electron transfer, but experimental data suggest a minor role. Also, we can rationalize the fact that Asp 34 (P) and Trp106 (P) are not involved in electron transfer and have an effect only in binding: they can easily be seen in Figure 3 as distant from the electron transfer pathway but still providing ionic bridges that can be important for binding.

**Table 3.** Kinetic Parameters for Cytochrome P450cam Reaction. WT and Mutant Protein Species[a]

| protein constituents | $V_{max}$ (nmol of NADH·nmol of CYP101·$s^{-1}$) | $K_m$ ($\mu$M) (CYP101) |
|---|---|---|
| WT Pdx−WT CYP101 | 23 | 0.30 |
| S44C Pdx−WT CYP101 | 28 | 0.76 |
| WT Pdx−L356A CYP101 | 21 | 0.26 |
| D38N Pdx−WT CYP101[12] | 12 | 5.96 |
| D34N Pdx−WT CYP101[12] | 22 | 0.65 |
| **protein constituents** | **$K_{et}$ ($s^{-1}$)** | **$K_d$ ($\mu$M) (CYP101)** |
| WT Pdx−WT CYP101[3] | 42 | 0.19 |
| WT Pdx−R112K CYP101[3] | 18 | 4.4 |
| WT Pdx−R112Y CYP101[3] | 0.16 | 110 |

[a] In these assays the concentration of CYP101 was varied and the parameters were calculated using nonlinear regression analysis of the hyperbolic curve resulting from the plot of activity vs CYP101 concentration. Data from our previous work[12] and from Unno et al.[3] are included for comparative purposes.

**Acknowledgment.** D.B. thanks the NIH for their grant (GM-48043). A.R. thanks Mike Gilson for interesting discussions on electrostatics and his help in using UHBD and Delphi, and Travis Gallagher for interesting discussions and help with some figures. Any commercial instruments, reagents, or materials are identified in this paper to adequately specify the experimental procedures. Such identification does not imply recommendation by the National Institute of Standards and Technology, nor does it imply that the materials are necessarily the best available for the purpose.

JA9739906

(42) Stayton, P. S.; Sligar, S. G. *Biochemistry* **1990**, *29*, 7381−.